Efficient Electrochemical Flow System with Improved Anode for the Conversion of CO_2 to CO

Journal of The Electrochemical Society, **161** (10) F1124-F1131 (2014)
0013-4651/2014/161(10)/F1124/8/$31.00 © The Electrochemical Society

Efficient Electrochemical Flow System with Improved Anode for the Conversion of CO_2 to CO

Sichao Ma,[a,b,*] Raymond Luo,[c] Saman Moniri,[c] Yangchun Lan,[c] and Paul J. A. Kenis[b,c,,z]**

[a]*Department of Chemistry, University of Illinois at Urbana-Champaign, Urbana, Illinois 61801, USA*
[b]*International Institute for Carbon Neutral Energy Research (WPI-I^{2}CNER), Kyushu University, Fukuoka, Japan*
[c]*Department of Chemical & Biomolecular Engineering, University of Illinois at Urbana-Champaign, Urbana, Illinois 61801, USA*

The electroreduction of CO_2 to CO or other products is one approach to curb the rise in atmospheric CO_2 levels and/or to store excess energy of renewable intermittent sources like solar and wind. To date most efforts have focused on improving cathode catalysis, despite other components such as the anode (oxygen evolution reaction, OER) also being of key importance. Here, we report that the dihydrate form of IrO_2 as the anode catalyst in alkaline media can achieve onset cell potentials as low as −1.55 V with a cathode overpotential of only 0.02 V, partial current densities for CO as high as 250 mA cm^{-2} (compared to ∼130 mA cm^{-2} with a Pt anode), and energy efficiencies as high as 70%. The IrO_2 non-hydrate proved to be much more durable by maintaining more than 90% of its activity after cycling the anode potential over the 0 to 1.0 V vs. Ag/AgCl range for over 200 times, whereas the dihydrate lost most of its activity after 19 cycles. Possible causes for these differences are discussed. This work shows that improvements to the anode, so to the OER, can drastically improve the prospects of the electrochemical reduction of CO_2 to useful chemicals.
 [DOI: 10.1149/2.1201410jes]

Manuscript submitted May 5, 2014; revised manuscript received July 28, 2014. Published August 6, 2014.

During the past several decades the atmospheric CO_2 levels have risen steadily, now reaching levels that have started to affect the global climate, as evident from global warming, rising sea levels and more erratic weather.[1–3] Multiple strategies, such as carbon capture and sequestration, increasing the energy efficiency of buildings and the transportation sector, and switching to energy sources that emit less CO_2 (i.e., natural gas or renewable source such as solar and wind, instead of coal) need to be employed simultaneously to curb this rise, hopefully leading to lower atmospheric CO_2 levels.[4] Apart from enhancing more efficient use of energy, use of renewable sources such as solar and wind is most desirable as they produce no CO_2.[4] However, both solar and wind are intermittent. Technologies for large scale energy storage or on-demand utilization, both of which are non-trivial at this time, are needed before the energy produced by these renewable sources can be exploited to the fullest extent.[5] Electrochemical reduction of CO_2 into value-added products may represent a means to store excess intermittent renewable energy while simultaneously recycling CO_2, thus assisting in building a low-carbon, or ideally carbon-neutral energy cycle.[6–13] Furthermore, utilizing CO_2 as a starting material for chemical production has the potential to reduce our dependency on fossil fuels.

Among the various products that can be produced by electrochemical reduction of CO_2, CO is attractive due to its versatility as a feedstock (with H_2) for the Fischer-Tropsch process, which enables the synthesis of a variety of chemical products.[14] To date, most studies on the electrochemical reduction of CO_2 to CO have focused on the performance of the cathode, resulting in partial current densities for CO (obtained by multiplying the total current density and the faradaic efficiency for CO(10)) up to about 120 mA cm^{-2} at applied cell potentials of up to −3 V under ambient conditions, as well as energy efficiencies between 30–70%.[15–25] For example, recently we reported on the development of a N-based Ag complex, which achieved comparable CO current density (110 mA cm^{-2}) as unsupported Ag catalysts, but with a much lower Ag loading.[19] We also studied the activity of Ag catalysts for CO_2 reduction to CO as a function of particle size and found that Ag catalyst with particle size at around 5 nm exhibits highest activity for CO_2 reduction.[20] Subsequently, we applied TiO_2 as a support to stabilize the Ag particles at a size that is very active, resulting in energy efficiency of 65% at −2 V cell potential and partial current density of 101 mA cm^{-2} at −3 V cell potential.[25] Higher partial current densities (*i.e.*, as high as 300 mA cm^{-2}) for CO only can be achieved under high pressure conditions (>15 atm) with cell potential more negative than −3 V.[26–28] For electrochemical CO_2 reduction to CO to become economically viable, high current densities (well above 200 mA cm^{-2}) need to be achieved simultaneously with overall system energy efficiency over ∼50% while operating at ambient conditions.[10,12,13]

The equilibrium cell potential for the electrochemical reduction of CO_2 to CO is −1.33 V, when the oxygen evolution reaction (OER) is the anode reaction.[29] However, a high overpotential is required to drive this process due to sluggish CO_2 reduction on the cathode as previously reported.[10,12,13,30] Previously, we successfully decreased the cell overpotential to less than 0.2 V by using an aqueous solution containing 1-ethyl-3-methylimidazolium tetrafluoroborate (EMIM BF_4) as a co-catalyst,[29] which presumably stabilizes a reaction intermediate.[31] However, the current density achieved with this system was quite low; less than 5 mA cm^{-2}.

While to date overcoming the sluggish reaction kinetics of CO_2 reduction on the cathode has been the main focus, the performance of the anode (OER) also plays a key role in determining overall system efficiency. To date the most widely used anode catalyst in electrochemical CO_2 reduction system has been Pt.[19,22,24,27,29,32–36] Pt, however, does not exhibit outstanding activity for the OER reaction and its performance is hampered by the potential for oxide formation.[37] Some researchers have tried alternative anode catalysts[16] or different anode reaction and anode catalyst combinations (e.g., hydrogen oxidation or Cl_2 formation instead of the OER)[36,38] with mixed success: the alternative OER catalyst was still not sufficiently active,[16] the setup became more complicated and more expensive chemicals were needed,[36] and more durable electrolyzer materials were needed to withstand the corrosive nature of the Cl_2 product.[38] Other work showed that the two major forms of iridium oxide (IrO_2), hydrate and non-hydrate, are among the most active catalysts for the OER in water electrolyzers due to the much lowered overpotentials compared to Pt or other transition metal oxides,[37,39–41] and differences in physical and chemical properties has been studied.[42–45] However, to date IrO_2 hydrate and non-hydrate have not been studied as anode catalysts in a CO_2 reduction electrolyzer.

Here we report on the use of the hydrate and non-hydrate forms of IrO_2 as anode catalysts in combination with high performance Ag cathodes for the efficient electrochemical reduction of CO_2 to CO in alkaline media, with the desire to achieve high selectivity and high current density for CO, in combination with high overall system efficiency through reducing overpotential on both the anode and the cathode. Also, we report on the origin of the observed differences in activity and durability between IrO_2 hydrate and non-hydrate forms.

*Electrochemical Society Student Member.
**Electrochemical Society Active Member.
zE-mail: kenis@illinois.edu

Experimental

Treatment and physical characterization of IrO_2 catalysts.— For most experiments, commercially available IrO_2 dihydrate (Premion, 99.99% metal basis, Alfa Aesar) and IrO_2 non-hydrate (Premion, 99.99% metal basis, Alfa Aesar) powders were used as received. To study the cause of the durability differences between IrO_2 dihydrate and non-hydrate, both IrO_2 dihydrate and non-hydrate were calcined in air for 30 min. at different temperatures (250, 350, 450, 550, and 650°C), using a tube furnace (Lindberg/Blue M, HTF55322A). The morphology of IrO_2 dihydrate catalysts before and after heat-treatment were examined using transmission electron microscopy (TEM, JOEL 2100 CRYO) operated at 200 kV. The TEM sample was prepared by placing a drop of the catalyst suspension in isopropanol onto a holey carbon-coated 200 mesh grid, followed by solvent evaporation. The crystalline structures of the different iridium oxide samples were obtained by X-ray diffraction (XRD) analysis using Siemens-Bruker D5000 diffractometer equipped with a CuKα source, and operated at 40 kV and 30 mA with a scan rate of 1 degree min^{-1}. In parallel these same samples were subjected to electrochemical measurements (see below). The Ir content in the exit electrolyte was determined by using ICP-OES (PerkinElmer-Optima 2000DV).

Electrochemical characterization of IrO_2 catalysts.—Electrode preparation.— The cathodes were prepared using an air-brush method as previously reported, using unsupported Ag nanoparticles (<100 nm particle size, 99.5% trace metals basis, Sigma-Aldrich).[22] Cathode catalyst inks were prepared by mixing Millipore water (200 μL), Ag catalyst (3.4 mg), Nafion solution (4.4 μL, 5 wt%, Fuel Cell Earth), and isopropyl alcohol (200 μL). The inks were then sonicated (Vibra-Cell ultrasonic processor, Sonics & Materials) for 15 minutes and air-brushed using the automated air-brushing deposition setup on a gas diffusion layer (GDL, Sigracet 35 BC gas diffusion layers, Ion Power) to create a gas diffusion electrode (GDE) covered with catalyst over a geometric area of 2.5 × 0.8 cm^2. A PTFE spacer with a 2.5 × 0.8 cm^2 window was placed on top of GDL during the deposition process to avoid catalyst being deposited outside of the expected area on the GDL. Since a fraction of the catalyst ended up on the spacer, or was left behind in the air-brush, we determined the actual loading by weighing the GDL before and after deposition. The weight loss was found to be on the order of 50% for the air-brushed cathodes. The anodes were prepared by hand-painting of IrO_2 catalyst inks comprised of Millipore water (200 μL), IrO_2 catalyst (2.5 mg), Nafion solution (6.5 μL, 5 wt%, Fuel Cell Earth), and isopropyl alcohol (200 μL). The inks (with IrO_2 dihydrate or non-hydrate) were sonicated for 15 minutes and then each painted on a gas diffusion layer (Sigracet 35 BC) over a geometric area of 1.0 × 2.5 cm^2 using a paintbrush. The cathodes had a catalyst loading of about 0.9 mg cm^{-2}, while all the anodes had a catalyst loading of 1 mg cm^{-2}.

Electrochemical flow reactor operation.—A flow reactor (reported previously[25,34]) in which a liquid electrolyte (here 1 M KOH) flows between the anode and cathode GDEs was used to perform the electrochemical reduction of CO_2 to CO. As in our prior work, a potentiostat (Autolab PGSTAT-30, EcoChemie) was used to control the cell potential in the potentiostatic electrolysis mode.[25] At times we controlled the total current in the galvanostatic electrolysis mode. In the potentiostatic mode, for each potential, the cell was allowed to reach steady state for 200 s, after which the gaseous product stream was analyzed using gas chromatography (Thermo Finnegan Trace GC). The current at a given condition was obtained by averaging the current over 180 s before stepping to the next potential. In the galvanostatic mode, the flow reactor was tested at total current of 10, 20, 40, 70, 100, or 150 mA. The reactor was allowed to reach steady state for about 200 s, after which the individual electrode potentials were recorded using multimeters (AMPROBE 15XP-B) connected to each electrode and a reference electrode (Ag/AgCl; RE-5B, BASi) placed in the electrolyte exit stream. The electrode potentials were corrected for IR drop as previously reported.[46] We found that the IR drop due to cell contact resistance (15 mV) is much smaller than the IR drop due to the resistance of the electrolyte (182 mV) at a cell potential of −3.00 V and associated resulting current of −261 mA (electrolyte resistance = 0.697 Ω). We used the same electrolyte resistance when correcting for IR drop at low current densities, because the electrolyte resistance will continue to be the dominating factor. Similarly, IR drop due to the cell contact resistance will be much smaller than the IR drop due to the electrolyte at lower currents. For the IR corrected data reported in Table I, we ignored the cell contact resistance. The complete calculations for IR drop can be found in the Supplementary Information (SI).[47] A mass flow controller (MASS-FLO, MKS instrument) was used to set the CO_2 (S.J. Smith Welding Supply) flow rate at 7 SCCM. A syringe pump (PHD 2000, Harvard Apparatus) supplied the 1 M KOH (Fisher Scientific, certified ACS pellets) electrolyte at 0.5 mL min^{-1}. The pH of the electrolyte was measured using a calibrated pH meter (Thermo Orion, 9106BNWP). A pressure controller (Cole-Parmer, 00268TC) downstream from the reactor was used to keep the gas pressure in reactor lower than the atmosphere, allowing gas

Table I. Faradaic efficiency for CO and H_2 for the experiments running at different currents using 3 anode catalysts: IrO_2 dihydrate, IrO_2 non-hydrate and Pt black (data obtained in galvanostatic mode).

Anode catalyst	Current density (mA/cm^2)	IR corrected potential (V)		Cell Potential (V)	faradaic efficiency (%)		Energy Efficiency (%)
		Cathode	Anode		CO	H_2	
IrO_2 dihydrate	10	−1.369	0.456	−1.83	90	9	70.89
	20	−1.442	0.484	−1.94	94	5	67.25
	40	−1.525	0.524	−2.08	97	1	62.55
	70	−1.591	0.578	−2.22	99	1	59.85
	100	−1.645	0.658	−2.37	98	1	55.31
	150	−1.751	0.774	−2.63	98	1	50.19
IrO_2 non-hydrate	10	−1.363	0.537	−1.91	88	4	64.19
	20	−1.435	0.571	−2.02	93	1	61.45
	40	−1.531	0.639	−2.20	93	1	56.87
	70	−1.639	0.734	−2.42	95	2	52.91
	100	−1.677	0.804	−2.55	98	2	51.95
	150	−1.768	0.963	−2.84	99	1	46.84
Pt black	10	−1.373	0.752	−2.13	87	1	55.19
	20	−1.448	0.830	−2.29	88	1	51.53
	40	−1.559	0.956	−2.54	89	2	47.20
	70	−1.648	1.111	−2.81	92	2	44.51
	100	−1.715	1.218	−3.00	96	2	43.25
	150	−1.848	1.423	−3.38	97	3	39.14

products formed on the catalyst surface of the GDE to leave through the GDE to the gas stream. Periodically, for product analysis, 1 mL of the effluent gas stream was sampled automatically and diverted into a gas chromatograph (Thermo Finnegan Trace GC) operating in the thermal conductivity detection (TCD) mode, with a Carboxen 1000 column (Supelco) and Helium as the carrier gas at a flow rate of 20 SCCM. The column was held at 150°C and the TCD detector was held at 200°C. The only cathode products detected by GC were CO and H_2 when using Ag as the catalyst, consistent with results reported previously.[21,28] For experiments conducted in the flow reactor, the onset potential is defined as the lowest cell potential at which we observe CO peak in GC. A fresh cathode was used for each flow reactor test.

Three-Electrode Cell Operation.—Cyclic Voltammetry (CV) was performed using a potentiostat (Autolab PGSTAT302N, EcoChemie), and a standard three-electrode cell with 1M KOH as the electrolyte. A catalyst-covered 3-mm glassy carbon disk rotating disk electrode (RDE; Metrohm 6.1204.300) as the working electrode, a Pt gauze (100 mesh, 99.9% metals basis, Sigma-Aldrich, 25*25 mm^2) as the counter electrode, and a Ag/AgCl as the reference electrode (RE-5B, BASi), separated from the working electrode by means of a Luggin capillary, were used. IrO_2 catalyst ink (4 μL) was deposited on the RDE and then dried under flowing Ar. The inks were prepared using the same method as described above for the GDE anodes. To determine catalyst activity, the potential was scanned from 0 to 0.8 V vs. Ag/AgCl at a scan rate of 25 mV s^{-1}, while for the stability test, the potential was continuously cycled between 0 and 1 V vs. Ag/AgCl at a scan rate of 100 mV s^{-1}. Ar gas was bubbled through the electrolyte for 15 min prior to all CV measurements. The RDE was rotated at 1600 rpm to eliminate mass transport issues and to remove any bubbles that form on the electrode surface during the experiment. For experiments conducted in a three-electrode cell (CV), the onset potential is defined as the working electrode potential at which the current reaches 0.2 mA.

Results and Discussion

Overpotential and current density.— The performance toward OER activity for the three anode catalysts, IrO_2 dihydrate, IrO_2 non-hydrate, and Pt black was studied using CV in a standard three-electrode cell. Both the IrO_2 dihydrate and IrO_2 non-hydrate catalysts achieved much higher current and significantly lower onset potential (> 0.2 V) for the OER compared to Pt black (Figure 1a), indicating that these two IrO_2 catalysts (dihydrate and non-hydrate) are more active than Pt black. The IrO_2 dihydrate catalyst performs slightly better: it exhibits a ∼50 mV earlier onset potential and a ∼4 mA higher current compared to the IrO_2 non-hydrate catalyst.

Next, we used an electrochemical flow reactor to determine whether the high activity of the IrO_2 catalysts observed in the three-electrode cell translates into good performance in an electrolyzer. GDEs with the two IrO_2 catalysts were prepared and compared with a Pt-covered GDE. The partial current density for CO (j_{co}) as a function of cell potential is shown in Figure 1b for the systems with these three anode catalysts. The electrolyzer performed significantly better when using one of the IrO_2 catalyst-based GDEs than when using the Pt catalyst-based GDEs. Specifically, at cell potentials of −2.75 V and −3 V, the improvement in j_{co} was more than 100 mA cm^{-2}. At −3 V cell potential, the system using IrO_2 dihydrate as the anode catalyst achieved a j_{co} as high as 250 mA cm^{-2}. To our knowledge this is the highest partial current density reported to date for the electroreduction of CO_2 to CO at ambient conditions. This level of performance enhances the probability of this technology being transitioned in an economically viable process.[12]

The CV data (Figure 1a) already indicates that the IrO_2-based anodes exhibit a low OER onset potential. To determine the onset potential for CO_2 reduction of the systems with different anode catalysts on GDEs, we analyzed the composition of the effluent gas stream of the flow reactor with GC for different cell potentials after the flow reactor reached steady state. Whereas no CO production was observed yet at a cell potential of −1.50 V, CO production was observed when applying −1.55 V cell potential (corresponding to an overpotential of only 0.22 V), when using IrO_2 dihydrate as the anode catalyst (Figure 1c). In comparison, the onset cell potential for CO production was −1.60 V (0.27 V overpotential) and −1.75 V (0.42 V overpotential) when respectively IrO_2 non-hydrate and Pt black were used as the anode catalyst. The overpotential for the system using IrO_2 dihydrate is 0.2 V lower than the system using Pt black as the anode, in agreement with the CV data shown in Figure 1a. In comparison to our previous work where we used an ionic liquid (EMIM BF_4) containing aqueous electrolyte to decrease the cell overpotential to less than 0.2 V,[29] here

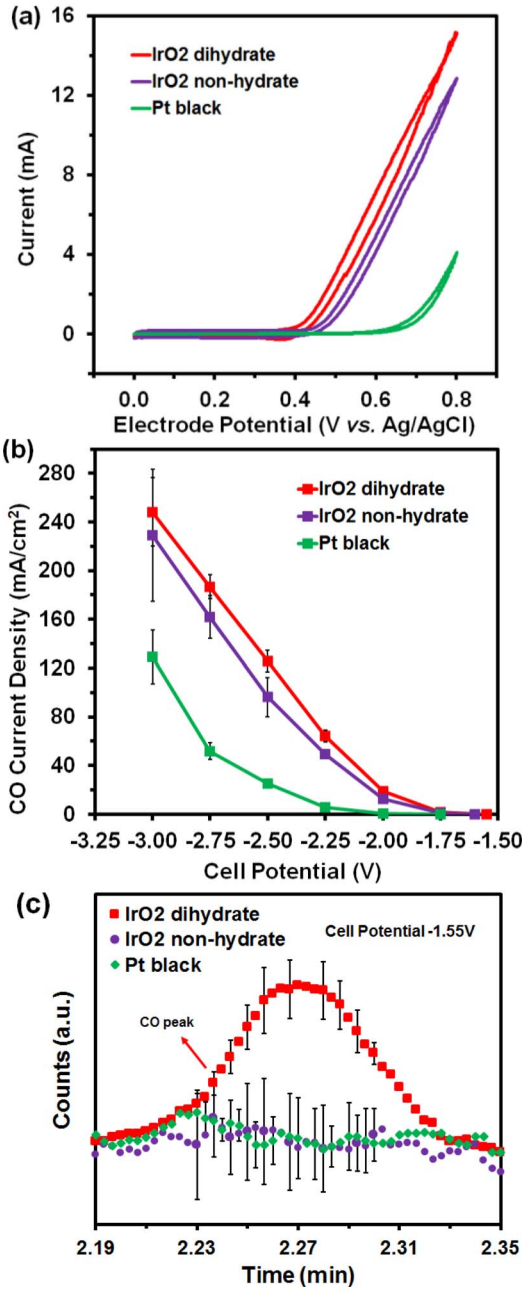

Figure 1. (a) CV measurements of IrO_2 dihydrate, IrO_2 non-hydrate and Pt black; (b) Partial current density for CO as a function of cell potential with IrO_2 hydrate, IrO_2 non-hydrate and Pt black as the anode catalysts (data obtained in potentiostatic mode); (c) GC peak at cell potential of −1.55 V applied on the electrochemical flow reactor with 3 different anode catalyst: IrO_2 dihydrate, IrO_2 non-hydrate and Pt black.

we are able to achieve a similar low cell overpotential (0.22 V) with an electrolyte that is much cheaper, less viscous (easier operation), and more conductive, resulting in higher throughput (current density).

The achieved low cell overpotential not only originates from the anode catalyst improvement, but is probably also due to the use of alkaline electrolyte. The standard potential for the cathode reaction

$$H_2O + CO_2 + 2e^- \rightarrow CO + 2OH^- \quad [1]$$

is calculated as follows: -0.109[7] – $0.0591 \times$pH (pH of 1M KOH is 13.48 from the pH measurement) – 0.209 (correction for reference electrode from SHE to Ag/AgCl) = −1.11 V vs. Ag/AgCl. At −1.55 V cell potential with IrO_2 dihydrate as the anode catalyst, the cathode potential was −1.13 V vs. Ag/AgCl. This correlates to a cathode overpotential of only 0.02 V, which is the lowest overpotential reported to date for the electrochemical reduction of CO_2 to CO on metal electrodes, lower than those reported for Au oxide derived catalysts in neutral electrolyte.[35] Compared to our prior work in which we used 18 mol% solutions of EMIM BF_4,[29] a much higher current density (129 mA cm^{-2} in this work vs. 3.9 mA cm^{-2} in prior work at −2.5 V cell potential) is obtained when using a Ag cathode and an IrO_2 dihydrate anode in the reactor filled with 1M KOH. Also, to compare the Ag cathode performance in 1M KOH and 1M KCl, we performed potentiostatic measurement in 1M KCl (pH = 6.62) using Ag cathode and IrO_2 non-hydrate anode. The results of the above experiment and potentiostatic measurements using 1M KOH in this study, as well as data from prior work[22] were summarized and compared in Figure S1 in the SI. As shown in Figure S1a, by changing the electrolyte (from 1M KCl to 1M KOH), the cathode polarization curves do not shift, while the anode polarization curves shift significantly, by as high as 0.5 V, mainly due to the effect of pH change on the standard potential of OER reaction (Figure S1a). The standard potential of OER will decrease by $0.0591 \times (13.48 - 6.62) = 0.41$ V when using 1M KOH instead of 1M KCl. The same is true for the CO_2 reduction to CO. However, the cathode polarization curves do not shift when changing electrolyte from 1M KCl to 1M KOH, indicating that the CO_2 reduction kinetics is improved in the alkaline solution. Therefore, a Ag cathode performs better in 1M KOH compared to 1M KCl as a result of a much lower overpotential in 1M KOH (0.41 V lower). When comparing the Ag cathodes in different electrolytes in Figure S1b this expected difference of 0.41V due to a change in pH cannot be seen, because all are plotted with respect to the Ag/AgCl reference electrode. The 1M KOH alkaline media increases the electrolyte conductivity (compared to $KHCO_3$ and K_2SO_4)[21] and may also improve the CO_2 reduction reaction kinetics due to the suppression of hydrogen evolution reaction by lowering H^+ concentration. Also, on the anode side, IrO_2 catalysts are more active in alkaline media than in other pH environment as previously reported.[44] Therefore, alkaline media not only works better for OER reaction on the anode, but also facilitates the CO_2 reduction reaction on the cathode, making it a highly suitable electrolyte for the electrochemical reduction of CO_2 to CO.

Energy efficiency and current-potential behavior.— The energy efficiency of an electrolysis process can be calculated using the following equation as previously reported:[12]

$$\varepsilon_{energetic} = \sum_k \frac{E_k^\circ \varepsilon_{k,Faradaic}}{E_k^\circ + \eta} = \sum_k \frac{E_k^\circ \varepsilon_{k,Faradaic}}{E_k^\circ + \eta_{cathode} + \eta_{anode}} \quad [2]$$

where E_k° is the equilibrium cell potential for a certain product, η is the cell overpotential, equal to the sum of the overpotentials from the cathode ($\eta_{cathode}$) and the anode (η_{anode}). In all experiments the two major products are H_2 and CO. No other products, which based on the faradaic efficiencies for H_2 and CO never totaled to a fraction higher than 5%, were detected. The equilibrium cell potential E^o for converting CO_2 to CO equals $E^o_{cathode} - E^o_{anode} = -0.10$ V -1.23 V $= -1.33$ V and for H_2 evolution E^o equals $E^o_{cathode} - E^o_{anode} = 0$ V -1.23 V $= -1.23$ V. $\varepsilon_{k,Faradaic}$ is the faradaic efficiency of product k and η is the cell overpotential (i.e., the sum of overpotentials on the cathode and anode).

To study how the system energy efficiency changes when using IrO_2 catalysts (dihydrate or non-hydrate) instead of Pt black, the flow reactor was operated in galvanostatic mode, in which the individual electrode potentials are measured when driving the cell with different currents (from 10 mA to 150 mA). Also note that to confirm the onset potential in potentiostatic mode, at current below 10 mA, we controlled cell potential for the systems with three different anode catalysts. Table I summarizes IR-corrected electrode potential and faradaic efficiency for CO (the desired product), and for H_2 (the by-product), as obtained for systems using IrO_2 dihydrate, IrO_2 non-hydrate, and Pt black. All cells used the same Ag cathode catalyst, so not surprisingly the three systems with different anode catalysts achieved similar, high faradaic efficiencies for CO: typically above 90% at the same current density, in agreement with prior studies.[19,25] In contrast, a significant increase in energy efficiency is observed when IrO_2 catalysts are used instead of Pt black (Figure 2a). Specifically, at a current density of 10 mA cm^{-2}, the system using IrO_2 dihydrate as the anode catalyst achieved an energy efficiency as high as 70%, compared to only 55% when using Pt black as the anode catalyst. Furthermore, when using IrO_2 dihydrate as the anode catalyst, even at a current density as high as 150 mA cm^{-2}, the energy efficiency was above 50%, compared to 39% when Pt black was used as the anode catalyst in this study. Also, the 50% energy efficiency at high current density observed here is higher than what has been reported previously. For example, Yamamoto et al. reported an energy efficiency of less than 30%,[16] while Dufek et al. reported an energy efficiency less than 40%,[18] both at total current densities of ≥150 mA cm^{-2}. In other studies energy efficiencies exceeding 60% have been reported, but typically at current densities less than 10 mA cm^{-2}.[25,29]

From the IR-corrected single electrode polarization curves (Figure 2b) it is clear that the improvements of the overall cell perfor-

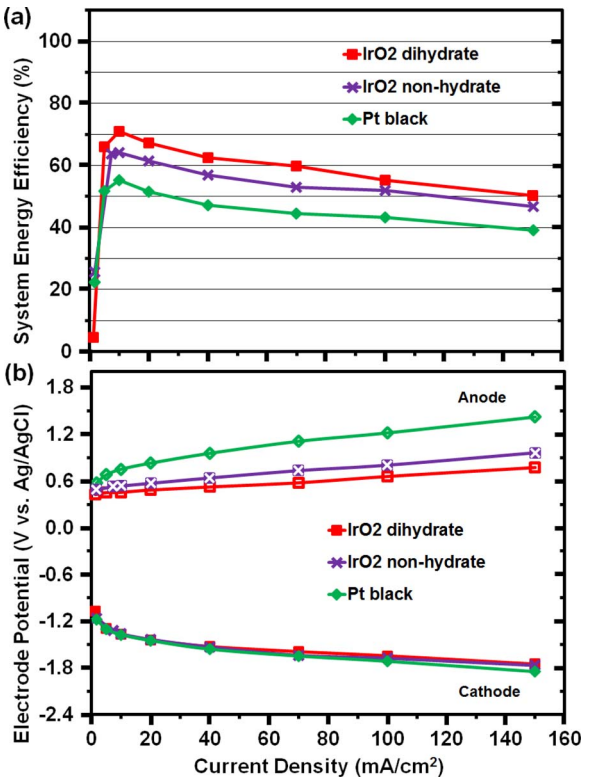

Figure 2. (a) Energy efficiency as a function of current density; (b) IR-corrected single electrode polarization curves of the experiments using 3 different anode catalysts: IrO_2 dihydrate, IrO_2 non-hydrate and Pt black (data obtained in galvanostatic mode).

mance (both energy efficiency and current density) can be attributed to the lower overpotentials exhibited by the anodes with IrO_2 catalysts compared to the ones with Pt catalyst. The improvement in anode overpotential was as high as 0.65 V at 150 mA cm^{-2} when IrO_2 dihydrate was used instead of Pt black. To no surprise, with all three systems using similar Ag cathodes, the cathode curves overlap almost completely. In sum, lower cell potentials were obtained by lowering the anode overpotential, which in turn has resulted in high energy efficiencies, even at high current densities.

The IR-corrected single electrode polarization curves (Figure 2b) also confirm the observations made using CV in a 3-electrode cell (Figure 1a): that the IrO_2 dihydrate catalyst exhibits a lower overpotential than the IrO_2 non-hydrate catalyst; in other words the dihydrate is better than the non-hydrate in terms of OER activity. To confirm the behavior of these IrO_2 catalysts under more conventional OER conditions, measurement under Ar-purged condition (flowing Ar instead of CO_2 in the cathode gas chamber during the experiment) was performed in the flow reactor (details shown in Section IV in the *SI*). This result shows that under the Ar flowing condition, IrO_2 dihydrate also performs better than IrO_2 non-hydrate toward the OER. In prior work the higher activity of IrO_2 hydrate compared to IrO_2 non-hydrate is attributed to the higher amount of surface hydroxyl species and highly dispersed amorphous structure of the IrO_2 hydrate, providing higher surface area, microporous morphology and more catalytic sites.[42–45]

Durability of the IrO_2 catalysts.— Although IrO_2 dihydrate exhibits a lower overpotential and thus achieves a higher current density compared to IrO_2 non-hydrate, the durability of these catalysts also needs to be investigated, as this property is of key importance when considering them for applications. Very little has been reported previously on the durability of these catalysts when used in alkaline solution. Here, we performed two different experiments to compare the durability of IrO_2 dihydrate and IrO_2 non-hydrate, one in a 3-electrode cell and one in the flow cell. First, continuous potential cycling (between 0 to 1V vs Ag/AgCl) was performed in a standard 3-electrode cell for both IrO_2 dihydrate and IrO_2 non-hydrate (Figures 3a and 3b). When using IrO_2 dihydrate, the current decreased significantly in successive cycles, overall from 35.28 mA to 1.78 mA after 19 cycles (Figure 3a). In contrast, when using IrO_2 non-hydrate, the current only decreased slightly in successive cycles, as evidenced in a drop of less than 2 mA (from 29.24 mA to 27.52 mA) after 200 cycles (Figure 3b).

Second, we also tested the durability of the two IrO_2 catalysts in the electrochemical flow reactor. The same anode was used for 4 – 5 trials in the flow reactor, which is operated in galvanostatic mode. The resulted steady state electrode potentials were recorded, and IR-corrected single electrode polarization curves were plotted in Figure 3(a′) and 3(b′). As shown in Figure 3(a′), the activity of IrO_2 dihydrate toward OER drops significantly after each trail test, while the IrO_2 non-hydrate anode is still as active as the fresh electrode after 5-trial test since the 5 anode polarization curves overlap (Figure 3(b′)), which is in good agreement with the results from continuous potential cycling experiment. Therefore, IrO_2 dihydrate is less durable compared to IrO_2 non-hydrate, which is probably due to anodic dissolution during the reaction as reported previously.[39,40,44,48]

In prior work the difference in durability between IrO_2 hydrate and non-hydrate has mainly been attributed to the difference in crystallinity and specific surface area.[42,48] To determine the effect of crystallinity on the durability, we collected XRD patterns of both IrO_2 dihydrate (Figure 4a) and IrO_2 non-hydrate (Figure 4b). This XRD data indicates that both the dihydrate and non-hydrate have a similar amorphous (non-crystalline) structure, so probably not the source of the observed differences in durability. The sharp peaks observed in the XRD patterns of both catalysts are due to the crystalline structure of Ir metal, which is a common component in commercial IrO_2 catalysts.[43] Since Ir will be oxidized to IrO_2 during reaction and both the dihydrate and non-hydrate are comprised of similar amounts of Ir, the presence of Ir (and the associated crystalline peaks in XRD) is assumed not to be the cause of the differences in durability and activity between these two catalysts.

Other causes for the observed difference in activity and durability between the two IrO_2 catalysts may originate from the amount of water content or the amount of surface hydroxyl species. To study how water content and surface species density affect catalysts durability, IrO_2 dihydrate and IrO_2 non-hydrate were both heat treated at 250, 350, 450, 550 and 650°C (Figures 4a and 4b). Upon gradual calcination of the catalysts, the water content, the coverage with

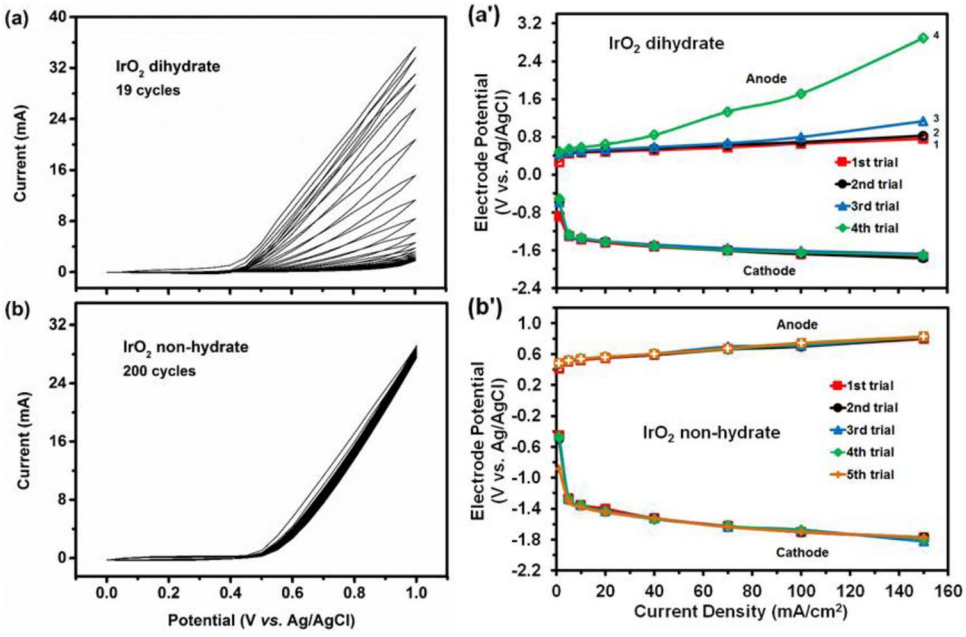

Figure 3. Left: Continuous potential cycling conducted in a standard 3-electrode cell for (a) IrO_2 dihydrate, and (b) IrO_2 non-hydrate. Electrolyte: 1M KOH; Scan rate: 100 mV/s; RDE rotating rate: 1600 rpm. Right: IR-corrected single electrode polarization curves for anode durability test conducted in an electrochemical flow reactor for (a′) IrO_2 dihydrate, and (b′) IrO_2 non-hydrate.

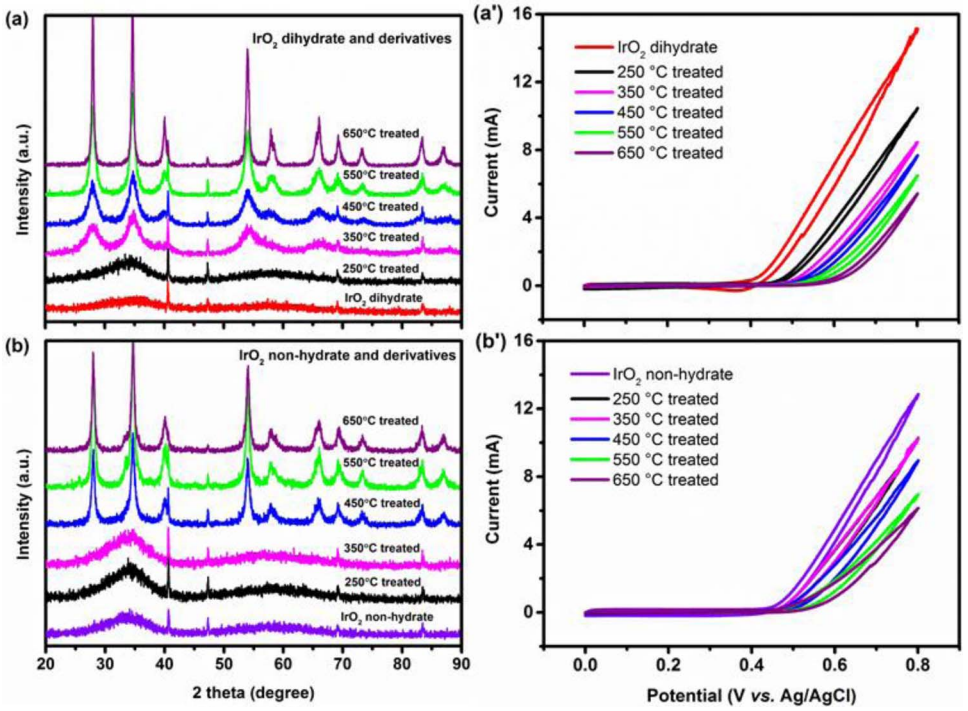

Figure 4. Left: XRD analysis of (a) IrO_2 dihydrate, and (b) IrO_2 non-hydrate upon thermal treatment. Right: CV measurements of (a′) IrO_2 dihydrate, and (b′) IrO_2 non-hydrate after thermal treatment at different temperatures. CV was conducted in 1M KOH at a scan rate of 25 mV/s, with the RDE rotating at 1600 rpm.

surface hydroxyl species, the morphology, as well as the crystallinity of the catalysts may change, which may help elucidate the connection between structure and electrochemical performance. For IrO_2 dihydrate, the structure changed from amorphous to crystalline at a temperature between 250 and 350°C (Figure 4a), while for IrO_2 non-hydrate, the transition happened between 350 and 450°C (Figure 4b). For both materials, the crystallinity increased when raising the temperature further, as evidenced by the sharpening of the peaks. The TEM micrographs shown in Figure S2[47] suggest that untreated (Figure S2b) and 250°C treated (Figure S2c) IrO_2 dihydrate have an amorphous structure with irregular particle shape. However, for IrO_2 dihydrate samples treated from 450°C to 650°C, the particles start to sinter (∼10 nm in Figure S2e to >20 nm in Figure S3g) and change shape to squares with more crystalline features, while the 350°C treated IrO_2 dihydrate sample (Figure S3d) appears to be in a state between amorphous and crystalline. These morphologies and trends observed in TEM are in agreement with the XRD results shown in Figure 4a. Figures 4(a′) and 4(b′) show the OER activity for samples of each of the two IrO_2 catalysts after treatment at different temperatures. Heat treatment leads to reduced OER activity for both IrO_2 dihydrate and IrO_2 non-hydrate, probably due to the loss of surface hydroxyl species, and/or a change of the crystalline structure and morphology (especially at temperatures above 350°C), leading to the decrease in electrochemical surface area of the catalyst. Further study of the durability of the 250°C treated IrO_2 dihydrate sample using continuous potential cycling (same experiment as used in Figures 3a and 3b) revealed that this sample is remarkably stable: the current dropped only by 12%, from 18.91 mA to 16.80 mA after 200 cycles. In contrast, recall that the untreated IrO_2 dihydrate sample loses more than 90% of its activity after only 19 cycles (Figure 3a), despite the XRD patterns (Figure 4a) and TEM micrographs (Figure S2b and S2c) of the untreated and the 250°C treated IrO_2 dihydrate samples being almost identical. This suggests that the difference in durability between the untreated and the 250°C treated IrO_2 dihydrate samples is probably due to the differences in water content or surface hydroxyl coverage, rather than due to a change in crystalline structure. Based on the above analysis, along with the observation from TEM (Figure S2a and S2b) that the 250°C treated IrO_2 dihydrate, the untreated IrO_2 non-hydrate, and the dihydrate samples have similar morphology, we conclude that the differences in activity and durability among these three IrO_2 catalysts can be attributed mainly to water content and/or surface hydroxyl coverage.

During the past few decades, a large amount of work has been done on OER, and several mechanisms were proposed.[37,44,49–54] Most of the mechanisms proposed for metal oxide catalysts include the formation and subsequent decomposition of higher valent metal oxides.[37,44,49] For example, according to Trassati et al.,[50] the mechanism would be as follows where S is an active site related to a topological defect on the catalyst:

$$S + OH^- \rightarrow S - OH + e^- \quad [3]$$

$$S - OH + OH^- \rightarrow S - O + H_2O + e^- \quad [4]$$

$$2S - OH \rightarrow S - O + S - H_2O \quad [5]$$

$$S - O + S - O \rightarrow O_2 + 2S \quad [6]$$

The Step 3 is followed by the formation of bounded oxide species, which then dissociates to oxygen.[37,49,50] Alternatively, the S-OH bond can be broken slowly to form a peroxide species, which dissociates to the solution (H_2O_2) or stays adsorbed on the surface (S-OOH), before decomposes to O_2.[52,54] Recently, DFT calculations have been reported and suggest that the OER mechanism consists of multiple single-electron charge-transfer steps with the involvement of three adsorbed intermediates: $OH_{(ad)}$, $O_{(ad)}$, and $OOH_{(ad)}$.[49,55,56] When correlating our results to the classic mechanism shown above (Step 3 to 6), we can consider Step 3 and 5 as the rate determining steps (RDS) on porous metal oxide materials such as the IrO_2 dihydrate used here, while Step 3 and 4 can be considered as the RDS on more dense species such as the IrO_2 non-hydrate used in this study. In this mechanism, the surface hydroxyl coverage is closely linked to the number of reaction sites since S-OH is the starting species in Step 4

and 5. More hydroxyls on the catalyst surface represents more reaction sites on the catalysts, which is probably why IrO_2 hydrate has more reaction sites than IrO_2 non-hydrate as previously reported.[42] When the reaction cycle starts, a higher hydroxyl surface coverage on IrO_2 dihydrate will facilitate Step 4 or 5 without the need to have Step 3 finish. For IrO_2 dihydrate, after faster consumption of hydroxyls, more empty sites will be created compared to IrO_2 non-hydrate, thereby increasing the reaction rate. Therefore, IrO_2 dihydrate initially exhibits a higher current density and lower overpotential because it has a higher hydroxyl surface coverage as well as more reaction sites compared to IrO_2 non-hydrate.[42] However, since hydroxyl species are involved in the oxidation of IrO_2 catalyst during the OER,[37] a higher amount of hydroxyls on the surface will also lead to higher possibility of further oxidation of IrO_2 and subsequent dissolution, lowering the durability of the dihydrate form. Indeed more Ir was detected using inductively coupled plasma optical emission spectroscopy in the electrolyte leaving the reactor when using the dihydrate catalyst (1.70 ppm when using dihydrate compared to 0.35 ppm when using non-hydrate). Our results and analysis reported here suggest that further experiments using in-situ spectroscopy in combination with theoretical and/or computational efforts are needed to further unravel the mechanistic aspects of the processes taking place on these electrodes, as also suggested previously.[49]

Conclusions

In summary, we studied IrO_2-based anode catalysts (a dihydrate and a non-hydrate form) for the oxygen evolution reaction in an electrochemical flow cell for the efficient reduction of CO_2 to CO on Ag cathodes. The use of the dihydrate form of IrO_2 instead of Pt black as the anode catalyst in 1M KOH lowered onset cell potential by ~0.2 V to −1.55 V. Also, this configuration produced the highest partial current densities for CO (250 mA cm^{-2}) reported to date under ambient conditions, compared to 130 mA cm^{-2} when Pt black was used as the anode catalyst. The use of 1 M KOH as the electrolyte helped improve the cathode reaction kinetics, as evidenced by a cathode overpotential of only 0.02 V, which to our knowledge is the lowest overpotential reported to date for the conversion of CO_2 to CO in aqueous media. These improvements result in an energy efficiency as high as 70% at 10 mA cm^{-2} and still >50% at 150 mA cm^{-2}.

While the initial performance of the two forms of IrO_2 catalysts, dihydrate and non-hydrate, was found to be similar, we found IrO_2 non-hydrate is much more durable (loses less than 10% of activity upon electrochemical cycling) than IrO_2 dihydrate (loses >90% of activity). Based on physical and electrochemical characterization of heat treated samples of the two IrO_2 catalysts, we concluded that these observed differences can be attributed to differences in their morphology, number of available active sites, and their ability to accommodate surface-bound hydroxyls.

While the use of IrO_2 anodes significantly improved the performance of electrochemical CO_2 conversion in a flow cell, further advances are needed to enhance the applicability of the process, specifically cathodes need to be developed that are able to achieve high energy efficiency (>50%) at much higher current density (>400 mA cm^{-2}) while maintaining high selectivity for a specific product, as well as electrodes that are able to handle the high mass transfer rates of the reactants and products. Further experimental and computational study of the reaction mechanism of CO_2 reduction in alkaline media is needed to understand the improved kinetics and may guide the design of yet better cathode catalysts.

Acknowledgment

We gratefully acknowledge financial support from the Department of Energy through an STTR grant to Dioxide Materials and UIUC (DE-SC0004453), and from the International Institute of Carbon Neutral Energy Research (WPI-I^2CNER), sponsored by the World Premier International Research Center Initiative (WPI), MEXT, Japan.

References

1. A. T. Bell, *Basic Research Needs, Catalysis for Energy*, U.S. Department of Energy: Bethesda (2008).
2. M. Z. Jacobson, *Energy Environ. Sci.*, **2**, 148 (2009).
3. P. Taylor, *Energy Technology Perspectives* International Energy Agency (2010).
4. S. Pacala and R. Socolow, *Science*, **305**, 968 (2004).
5. N. S. Lewis, *Science*, **315**, 798 (2007).
6. M. Gattrell, N. Gupta, and A. Co, *J. Electroanal. Chem.*, **594**, 1 (2006).
7. C. Oloman and H. Li, *Chemsuschem*, **1**, 385 (2008).
8. Y. Hori, in *Handbook of Fuel Cells*, p. 720, John Wiley & Sons, Ltd (2010).
9. M. Mikkelsen, M. Jorgensen, and F. C. Krebs, *Energy Environ. Sci.*, **3**, 43 (2010).
10. D. T. Whipple and P. J. A. Kenis, *J. Phys. Chem. Lett.*, **1**, 3451 (2010).
11. B. Kumar, M. Llorente, J. Froehlich, T. Dang, A. Sathrum, and C. P. Kubiak, *Annu. Rev. Phys. Chem.*, **63**, 541 (2012).
12. H.-R. M. Jhong, S. Ma, and P. J. A. Kenis, *Curr. Opin. Chem. Eng.*, **2**, 191 (2013).
13. A. M. Appel, J. E. Bercaw, A. B. Bocarsly, H. Dobbek, D. L. DuBois, M. Dupuis, J. G. Ferry, E. Fujita, R. Hille, P. J. A. Kenis, C. A. Kerfeld, R. H. Morris, C. H. F. Peden, A. R. Portis, S. W. Ragsdale, T. B. Rauchfuss, J. N. H. Reek, L. C. Seefeldt, R. K. Thauer, and G. L. Waldrop, *Chemical Reviews*, **113**, 6621 (2013).
14. M. E. Dry, *Catal. Today*, **71**, 227 (2002).
15. Y. Hori, H. Wakebe, T. Tsukamoto, and O. Koga, *Electrochim. Acta*, **39**, 1833 (1994).
16. T. Yamamoto, D. A. Tryk, A. Fujishima, and H. Ohata, *Electrochim. Acta*, **47**, 3327 (2002).
17. C. Delacourt, P. L. Ridgway, J. B. Kerr, and J. Newman, *J. Electrochem. Soc.*, **155**, B42 (2008).
18. E. Dufek, T. Lister, and M. McIlwain, *J. Appl. Electrochem.*, **41**, 623 (2011).
19. C. E. Tornow, M. R. Thorson, S. Ma, A. A. Gewirth, and P. J. A. Kenis, *J. Am. Chem. Soc.*, **134**, 19520 (2012).
20. A. Salehi-Khojin, H.-R. M. Jhong, B. A. Rosen, W. Zhu, S. Ma, P. J. A. Kenis, and R. I. Masel, *J. Phys. Chem. C*, **117**, 1627 (2012).
21. E. J. Dufek, T. E. Lister, and M. E. McIlwain, *Electrochem. Solid-State Lett.*, **15**, B48 (2012).
22. H.-R. M. Jhong, F. R. Brushett, and P. J. A. Kenis, *Advanced Energy Materials*, **3**, 589 (2013).
23. M. R. Thorson, K. I. Siil, and P. J. A. Kenis, *J. Electrochem. Soc.*, **160**, F69 (2013).
24. K. P. Kuhl, E. R. Cave, D. N. Abram, and T. F. Jaramillo, *Energy Environ. Sci.*, **5**, 7050 (2012).
25. S. Ma, Y. Lan, G. M. J. Perez, S. Moniri, and P. J. A. Kenis, *Chemsuschem*, **7**, 866 (2014).
26. M. Todoroki, K. Hara, A. Kudo, and T. Sakata, *J. Electroanal. Chem.*, **394**, 199 (1995).
27. K. Hara and T. Sakata, *Bull. Chem. Soc. Jpn.*, **70**, 571 (1997).
28. E. J. Dufek, T. E. Lister, S. G. Stone, and M. E. McIlwain, *J. Electrochem. Soc.*, **159**, F514 (2012).
29. B. A. Rosen, A. Salehi-Khojin, M. R. Thorson, W. Zhu, D. T. Whipple, P. J. A. Kenis, and R. I. Masel, *Science*, **334**, 643 (2011).
30. Y. Hori, in *Modern Aspects of Electrochemistry*, C. Vayenas, R. White, and M. Gamboa-Aldeco Editors, p. 89, Springer New York (2008).
31. B. A. Rosen, J. L. Haan, P. Mukherjee, B. Braunschweig, W. Zhu, A. Salehi-Khojin, D. D. Dlott, and R. I. Masel, *J. Phys. Chem. C*, **116**, 15307 (2012).
32. N. Furuya and K. Matsui, *Journal of Electroanalytical Chemistry and Interfacial Electrochemistry*, **271**, 181 (1989).
33. M. Schwartz, M. E. Vercauteren, and A. F. Sammells, *J. Electrochem. Soc.*, **141**, 3119 (1994).
34. D. T. Whipple, E. C. Finke, and P. J. A. Kenis, *Electrochem. Solid-State Lett.*, **13**, B109 (2010).
35. Y. Chen, C. W. Li, and M. W. Kanan, *J. Am. Chem. Soc.*, **134**, 19969 (2012).
36. J. Wu, F. G. Risalvato, P. P. Sharma, P. J. Pellechia, F.-S. Ke, and X.-D. Zhou, *J. Electrochem. Soc.*, **160**, F953 (2013).
37. S. Park, Y. Shao, J. Liu, and Y. Wang, *Energy Environ. Sci.*, **5**, 9331 (2012).
38. T. E. Lister and E. J. Dufek, *Energy Fuels*, **27**, 4244 (2013).
39. E. Guerrini, H. Chen, and S. Trasatti, *J. Solid State Electrochem.*, **11**, 939 (2007).
40. M. Carmo, D. L. Fritz, J. Mergel, and D. Stolten, *Int. J. Hydrogen Energy*, **38**, 4901 (2013).
41. C. C. L. McCrory, S. Jung, J. C. Peters, and T. F. Jaramillo, *J. Am. Chem. Soc.*, **135**, 16977 (2013).
42. I. D. Belova, T. V. Varlamova, B. S. Galyamov, Y. E. Roginskaya, R. R. Shifrina, S. G. Prutchenko, G. I. Kaplan, and M. A. Sevostyanov, *Mater. Chem. Phys.*, **20**, 39 (1988).
43. J. C. Cruz, V. Baglio, S. Siracusano, R. Ornelas, L. Ortiz-Frade, L. G. Arriaga, V. Antonucci, and A. S. Aricò, *J Nanopart Res*, **13**, 1639 (2011).
44. A. Minguzzi, F.-R. F. Fan, A. Vertova, S. Rondinini, and A. J. Bard, *Chemical Science*, **3**, 217 (2012).
45. H. A. Elsen, C. F. Monson, and M. Majda, *J. Electrochem. Soc.*, **156**, F1 (2009).
46. M. S. Naughton, A. A. Moradia, and P. J. A. Kenis, *J. Electrochem. Soc.*, **159**, B761 (2012).
47. S. Ma, R. Luo, S. Moniri, Y. Lan, and P. J. A. Kenis, *Supplementary Information*.
48. S. Song, H. Zhang, X. Ma, Z. Shao, R. T. Baker, and B. Yi, *Int. J. Hydrogen Energy*, **33**, 4955 (2008).

49. H. Dau, C. Limberg, T. Reier, M. Risch, S. Roggan, and P. Strasser, *ChemCatChem*, **2**, 724 (2010).
50. G. Lodi, E. Sivieri, A. De Battisti, and S. Trasatti, *J. Appl. Electrochem.*, **8**, 135 (1978).
51. S. Trasatti, *Electrochim. Acta*, **29**, 1503 (1984).
52. J. O. Bockris and T. Otagawa, *J. Phys. Chem.*, **87**, 2960 (1983).
53. J. O. M. Bockris and T. Otagawa, *J. Electrochem. Soc.*, **131**, 290 (1984).
54. S. P. Mehandru and A. B. Anderson, *J. Electrochem. Soc.*, **136**, 158 (1989).
55. J. Rossmeisl, Z. W. Qu, H. Zhu, G. J. Kroes, and J. K. Nørskov, *J. Electroanal. Chem.*, **607**, 83 (2007).
56. J. Rossmeisl, A. Logadottir, and J. K. Nørskov, *Chem. Phys.*, **319**, 178 (2005).